J Nanostruct 16(2): 1500-1507, Spring 2026

RESEARCH PAPER

Magnetic Iron Oxide Nanoparticles of Antibacterial Activities Study and Characterization Physics Properties

Rusul K. Ismail [1], Shahlaa M. Abd Al-Hussan [2], Noor H. Kurshed [3]*

[1] College of Dentistry, University of Diyala, Ba'aqubah, Diyala, 32001, Iraq

[2] Ministry of Education. Diyala Education Directorate, Diyala, 32001, Iraq

[3] Department of Soil, College of Agriculture, University of Diyala, Ba'aqubah, Diyala, 12, Iraq

ARTICLE INFO

Article History:
Received 09 December 2025
Accepted 07 February 2026
Published 01 April 2026

Keywords:
Antibacterial
Co-Precipitation
Fe_3O_4 NPs
Iron Oxide
Nanoparticles

ABSTRACT

This paper describes the co-precipitation manufacture of magnetite iron oxide nanoparticles (Fe_3O_4 NPs). Using Fourier Transform Infrared (FT-IR) spectrophotometry, X-Ray Diffraction (XRD), Dynamic Light Scattering (DLS) analysis, and Field Emission Scanning Electron Microscopy (FESEM) equipment, the structure, morphology, and magnetic characteristics of the produced material were described. The FT-IR spectrum offers crucial proof of the magnetite (Fe_3O_4) nanoparticles' effective production and provides important details about the functional groups connected to the nanoparticle surface. The Scherer's Formula determined the average particle size of 15.7 nm based on the XRD result, which showed the existence of Fe_3O_4 NPs. The XRD pattern matched the reference magnetite (Fe_3O_4) pattern (JCPDS No.19-0629). The sample displayed a monodisperse distribution profile with a single dominant peak, indicating a homogenous population of particles. The diffraction light scattering (DLS) particle size analyzer revealed an average size of iron oxide nanoparticles. Iron oxide nanoparticles' cubical to sub-cubical structure, reasonably uniform morphology, and average size of 52.5 nm were validated by characterization of their mean particle size and shape. Fe_3O_4 NPs' antibacterial properties were assessed by determining their minimum inhibitory concentration (MIC). Active antibacterial action against bacterial species was demonstrated by Fe_3O_4 NPs, with MICs values of 25 mg/ml for K. pneumonia and 50 mg/ml S. aureus and E. coli.

How to cite this article
Ismail K., Al-Hussan S., Kurshed N. Magnetic Iron Oxide Nanoparticles of Antibacterial Activities Study and Characterization Physics Properties. J Nanostruct, 2026; 16(2):1500-1507. DOI: 10.22052/JNS.2026.02.001

INTRODUCTION

Since nanotechnology manipulates matter at a scale where materials exhibit distinct and desirable properties from those at the micro-macro scale, it has emerged as one of the most important components of scientific expertise. It has garnered a lot of interest, especially in the field of medical research, which has a significant impact on the world economy. Particles that range in size from 1 to 1000 nm are known as nanoparticles [1,2]. The biological industry frequently uses them because of their better qualities than sheer-sized particles, such as their new optical features, strong magnetic characteristics, high activity, and greater surface-to-volume ratio. Nanoparticles have a broad range of applications in biomolecules

* Corresponding Author Email: shahlamn91@yahoo.com

and cells. Nanoparticles' aggregation, charge, crystalline structure, chemical makeup, size, shape, and solubility all affect this interaction [3–5]. The most widely used of these in bioanalytical methods and biomedical applications are magnetic nanoparticles. Biotype specimens are less affected by background interference; hence the magnetic susceptibilities of biotype samples are almost negligible. The external magnetic field can readily reach biological samples because of this benefit [6,7]. These days, a wide variety of biomedical applications, including: (analytical tools, bioimaging, biosensors, contrast agents (CAs), hyperthermia, photoablation therapy, physical therapy applications, separation, signal markers, and targeted drug delivery (TDD)), can be designed to integrate magnetic nanoparticles [1–8]. Because of their high saturation magnetization, high magnetic susceptibility, chemical stability, and innocuousness, iron oxide nanoparticles (IONPs) were utilized in the majority of research. Nickel and cobalt are examples of IONPs with strong magnetic characteristics that oxidize readily and are poisonous. In biomedical applications, magnetite (Fe_3O_4) nanoparticles (MNPs) are the most often used IONPs [4]. The transition of ions from Fe^{2+} ions to Fe^{3+} ions results in the unique electrical and magnetic properties of magnetite nanoparticles.

MNPs with superparamagnetism characteristics are often employed in the biomedical industry and are less than 20 nm. In addition, they are used extensively in this sector in comparison to other magnetic-IONPs (M-IONPs) because of their superparamagnetism feature, narrowed particle size distribution (<100 nm), high magnetization saturation value, and biocompatible surface chemistry [8–10]. Of the (M-IONPs), magnetite (Fe_3O_4), maghemite (γ-Fe_2O_3), and hematite (α-Fe_2O_3) are the three most common types. The most stable chemical molecule in the presence of air for an extended length of time is hematite (α-Fe_2O_3). Nevertheless, of the two (M-IONPs) stated, hematite (α-Fe_2O_3) has the lowest magnetic strength. Magnetite (Fe_3O_4) oxidizes to generate the phase known as maghemite (γ-Fe_2O_3) [2,4,11]. The word "magnetite" comes from the name of the Asia Minor province of Magnesia, where massive deposits of magnetite were found. Because magnetite contains ferric (oxidized) and ferrous (reduced) iron atoms, it is also frequently inferred to be iron (III) oxide [12]. The chemical makeup of the molecule is depicted below to show a typical magnetite production reaction:

FeO (Ferrous Oxide) + Fe_2O_3 (Ferric Oxide) → Fe_3O_4 Magnetite

The kind of iron oxide—trivalent or divalent—determines the type of magnetite. The magnetite stoichiometric of Fe^{2+}: Fe^{3+} is 1:2, and Zn, Mn, Co, and other divalent ions can either fully or partially replace divalent irons. As a result, magnetite may exhibit n-type or p-type semiconductor behavior [13]. Although a number of ways have been established to synthesize MNPs, the three main methodologies are wet chemical, physical, and microbiological methods. Every route has unique benefits, drawbacks, and impacts on various MNP attributes [14]. Due to its ease of use and effectiveness, the co-precipitation method is one of the most used techniques for creating aqueous phases [10]. Massart et al. initially developed this technique in 1981 [15]. Usually, metal precursors are alkalized to carry it out. The most well-known is the aging of ferrous and ferric salts in a NaOH base at room temperature and with a constant flow of inert gas at a 1:2 stoichiometric ratio. Following reaction describes a typical example of magnetite production (Fe_3O_4) [16]:

$$Fe^{2+} + 2Fe^{3+} + 8OH^- \rightarrow Fe(OH)_2 + 2Fe(OH)_3 \rightarrow Fe_3O_4 + 4H_2O$$

Two separate stages are used in the co-precipitation approach to produce homogenous nanoparticles: (i) nucleation and (ii) growth [17,18]. Crystalline particles typically begin the nucleation phase by precipitating from a supersaturated solution until the number of constituent species drops, resulting in the formation of nanoparticle crystals. The solute diffuses from the solution to the crystal surface during the slow-controlled growth phase, whereas the nucleation process lasts for a relatively brief duration. The production of extremely monodispersed MNPs might be achieved by controlling and separating the two phases, that is, by preventing nucleation and crystal growth from happening at the same time.

If the nuclei start to develop simultaneously, the particle nuclei may expand in a very limited distribution. Because the acquired particle size does not change during the growth phase, it could only be adjusted during the nucleation phase

[16,19]. The co-precipitation method was used in this study to create iron-oxide nanoparticles, which were then characterized using: (field emission scanning electron microscopy (FESEM), Fourier Transform Infra-Red (FT-IR) spectrophotometry, dynamic light scattering (DLS) analysis, and X-Ray diffraction (XRD)). The antibacterial qualities of iron oxide magnetic nanoparticles (Fe_3O_4 NPs) against human pathogenic bacteria, particularly S. aureus, E. coli, and K. pneumoniae, are being investigated.

MATERIALS AND METHODS

Materials Required

Ferrous Sulfate Heptahydrate ($FeSO_4.7H_2O$), Ferric Chloride Hexahydrate ($FeCl_3.6H_2O$), ammonium hydroxide solution (NH_4OH), ethanol (C_2H_5OH), and deionized water are all supplied by LOBA CHEMIE PVT.LTD. in India. Diyala University in Iraq's Medical Biology Lab., Dentistry College, provided the cultures of S. aureus, E. coli, and K. pneumoniae.

Preparation of Fe_3O_4 NPs

Co-precipitation of ferrous and ferric ion salts in aqueous solution was accomplished by adding base at room temperature while N_2 gas flowed. In summary, 0.2M of $FeSO_4.7H_2O$ and 0.1M of $FeCl_3.6H_2O$ were added to an aqueous solution in deionized water while being vigorously stirred at 1000 rpm. NH_4OH was then added to achieve a pH of 10. After that, it was filtered and repeatedly cleaned with deionized water until the pH was neutral. Fe_3O_4 was then cleaned with ethanol and dried. The powder It was gathered for antibacterial use and characterisation. Following reaction provides the following expression for the pertinent chemical reaction:

$$2FeCl_3.6H_2O + FeSO_4.7H_2O\ 8NH_4OH \rightarrow Fe_3O_4 + (NH_4)_2SO_4 + 6NH_4Cl + 19H_2O$$

Antibacterial Activities

A stock solution of the antimicrobial agent was prepared at a concentration higher than the expected MIC, followed by serial (100 mg/ml, 50 mg/ml. 25 mg/ml, 12.5 mg/ml, 6.25 mg/ml, 3.125 mg/ml and 1.562 mg/ml, respectively) two-fold dilutions in Mueller-Hinton broth (1 mL per sterile test tube). The bacterial isolate was cultured on a fresh agar plate (18–24 h), and colonies were suspended in sterile saline to match 0.5 McFarland standard (~1.5×10^8 CFU/mL), then diluted 1:100 to achieve ~5×10^5 CFU/mL. Each tube received 100 µL of the inoculum, resulting in a final bacterial density of ~5×10^5 CFU/mL. The tubes were incubated aerobically at 35 ± 2 °C for 16–20 h without shaking. After incubation, tubes were examined for turbidity, and the MIC was recorded as the lowest concentration showing no visible growth.

RESULTS AND DISCUSSION

Fourier-transform infrared spectroscopy (FTIR)

Fig. 1 displays the chemically produced iron oxide sample's FTIR spectrum. The spectrum offers

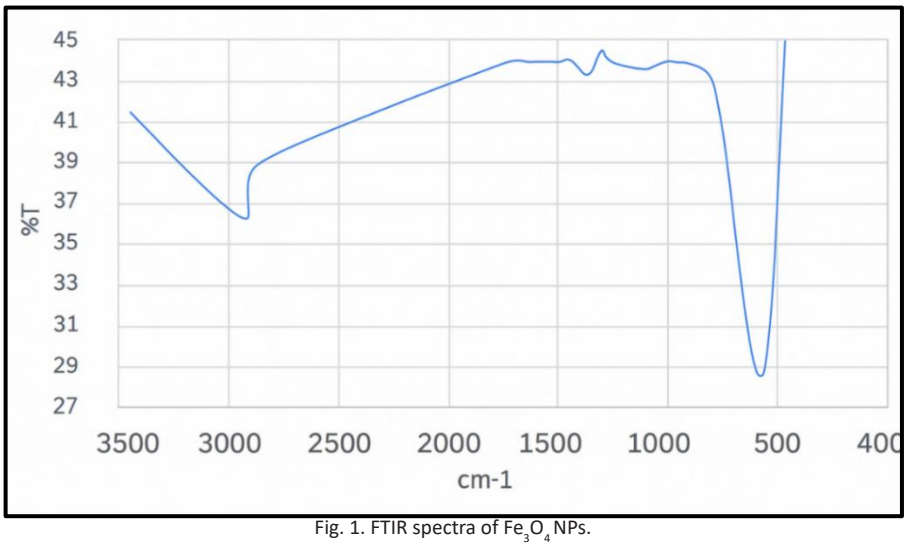

Fig. 1. FTIR spectra of Fe_3O_4 NPs.

crucial proof that magnetite (Fe_3O_4) nanoparticles were successfully formed and provides important details on the functional groups connected to the nanoparticle surface. Around 570 cm^{-1}, a noticeable absorption band is seen, which is associated with the Fe–O bond's stretching vibration. This peak validates the creation of crystalline Fe_3O_4 nanoparticles and is a distinctive fingerprint of the spinel structure of magnetite. This peak's existence confirms that the intended nanostructure was successfully synthesized [20–22]. The 1000–1500 cm^{-1} range also shows a number of weaker bands, which are often ascribed to C–O stretching, C–H bending, or C=C skeletal vibrations [23]. The presence of these functional groups which could be the result of residual organic compounds used during synthesis, such as surfactants, solvents, or stabilizing agents—indicates that some organic molecules remained on the surface of the nanoparticles, potentially serving as capping layers that prevent agglomeration. The spectrum also shows a notable dip in the 2900–3000 cm^{-1} region, which corresponds to aliphatic C–H stretching vibrations, which further supports the involvement of organic stabilizers or carbon-containing residues adsorbed on the surface of the nanoparticles. Curiously, the broad O–H stretching band, which is normally found between 3200 and 3600 cm^{-1}, is not prominently visible in this spectrum [23]. This indicates a comparatively dry surface with few hydroxyl functional groups or adsorbed moisture, maybe as a result of efficient drying or heat treatment procedures used in sample preparation. All things considered, the FTIR measurement shows the existence of surface-bound organic groups and validates the creation of Fe_3O_4 nanoparticles. These results are in line with the chemical synthesis procedure and lend credence to the theory that the final nanoparticles have a core-shell structure, consisting of an organic-coated surface and a magnetic iron oxide core, which may affect their stability, dispersibility, and capacity for additional functionalization in environmental or biomedical applications.

X-ray diffraction (XRD)

Fig. 2 displays the phase purity and crystallinity of the produced Fe_3O_4 NPs. The crystalline planes (111), (220), (311), (400), (422), (511), and (440) are represented by the XRD signals of Fe_3O_4 NPs at 21.3384˚, 30.4482˚, 35.8449˚, 43.5486˚, 53.6550˚, 57.5956˚, and 63.3057˚, respectively. These signals demonstrate the crystalline cubic structure of the magnetite phase (Fe_3O_4) (JCPDS No.19-

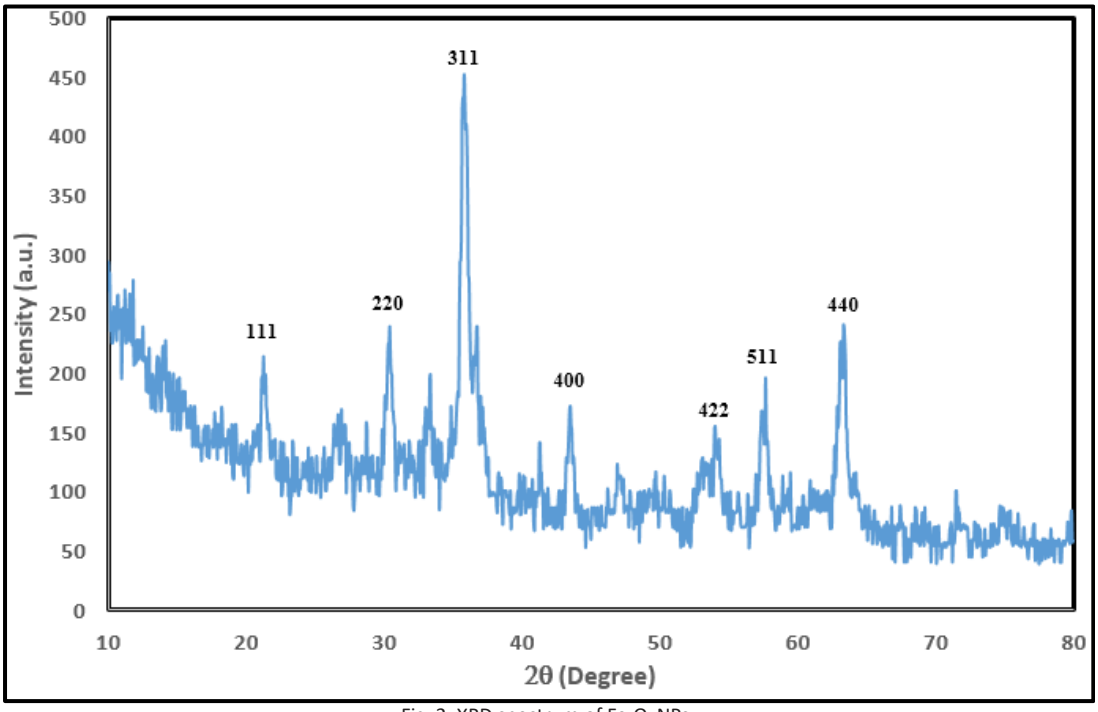

Fig. 2. XRD spectrum of Fe_3O_4 NPs.

0629). After taking instrumental broadening into consideration, the Debye-Scherrer formula was used to determine the crystallite size of the nanocrystalline materials based on X-ray line broadening studies (Eq. 1) [24,25].

$$D_{hkl} = \frac{K\lambda}{\beta\cos\theta} \quad (1)$$

where K (0.94) is a dimensionless value and D is the XRD crystallite size in nm. The X-ray radiation wavelength for Cu Kα (0.15406 nm) is denoted by λ, the Bragg angle by θ, and the line broadening at half the maximum intensity (FWHM in radians on the 2θ scale) by β. The full-width at half maximum of the (311) plane at (2θ = 35.8449˚) was used to compute the average particle size of synthesized Fe_3O_4 NPs, which came out to be 15.7 nm [26].

Bragg's law (Eqs. 2 and 3) determines the lattice parameter "a" and the interplanar spacing dhkl [27].

$$d_{hkl} = \frac{\lambda}{2\sin\theta} \quad (2)$$

$$d_{hkl} = \frac{a}{\sqrt{h^2 + k^2 + l^2}} \quad (3)$$

Additionally, for the produced Fe_3O_4 NPs, the interplanar spacing is d_{311} = 2.5044, and the lattice parameter is a = 8.3060A˚. Compared to the stated values for bulk magnetite (JCPDS No.19-0629), the predicted values for (a and d_{311}) are rather similar.

Dynamic Light Scattering (DLS)

Using Dynamic Light Scattering (DLS) examination on the HORIBA SZ-100 particle size analyzer, the hydrodynamic diameter of the produced Fe_3O_4 nanoparticles was ascertained. A homogenous population of particles was indicated by the sample's monodisperse distribution profile, which included a single dominant peak. As shown in Fig. 3, the average particle size was 127.7 nm, with a modal diameter of 125.4 nm and a standard deviation of 33.6 nm. A rather narrow size distribution was indicated by the Z-average value of 101.8 nm and the Polydispersity index (PDI) of 0.401, which were both determined by cumulated analysis. The study was carried out with a scattering angle of 90° and at 25.1°C. The viscosity of the dispersion medium was 0.893 mPa. Fe_3O_4 nanoparticle production at the nanoscale, which is essential for biomedical and environmental applications, as demonstrated by DLS data [28]. For applications requiring stability and controlled

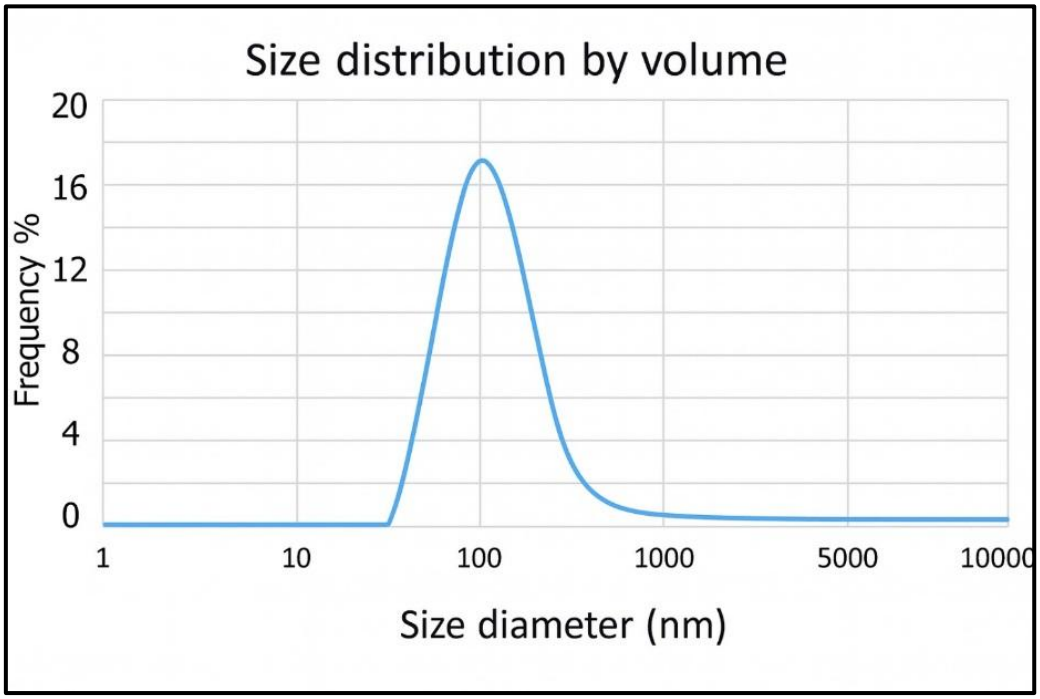

Fig. 3. DLS particle size analysis curve of Fe_3O_4 NPs.

diffusion, such as magnetic targeting, drug delivery, and biosensing, an average size of around 127 nm is perfect. For consistent physicochemical behavior, the sample's monodisperse nature and good PDI value (<0.5) suggest a well-dispersed system with negligible aggregation. Although there is a little number of bigger particles present, the sample's homogeneity is unaffected significantly by the slightly larger mean size in comparison to the Z-average. These results are in line with prior studies that describe stable Fe_3O_4 nanoparticle systems made with green or chemical methods. They offer a strong foundation for ensuing functionalization or surface modification

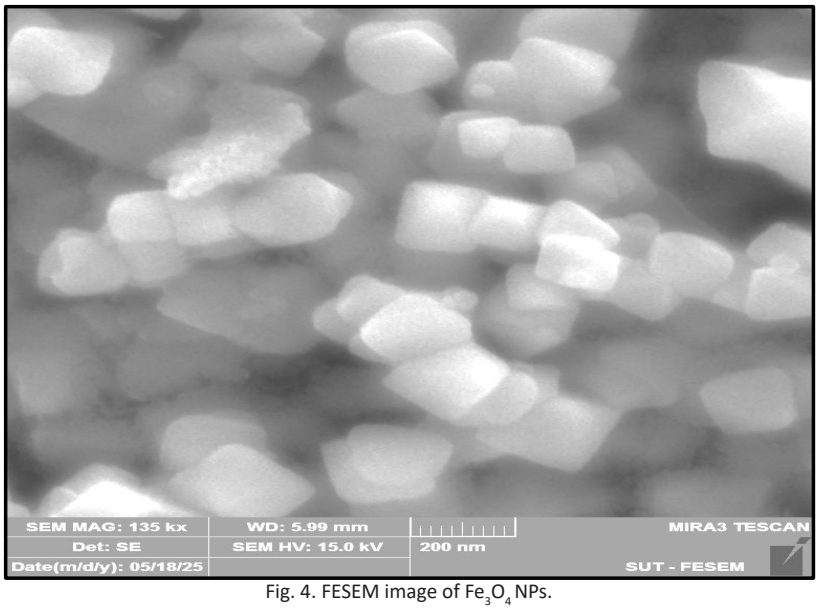

Fig. 4. FESEM image of Fe_3O_4 NPs.

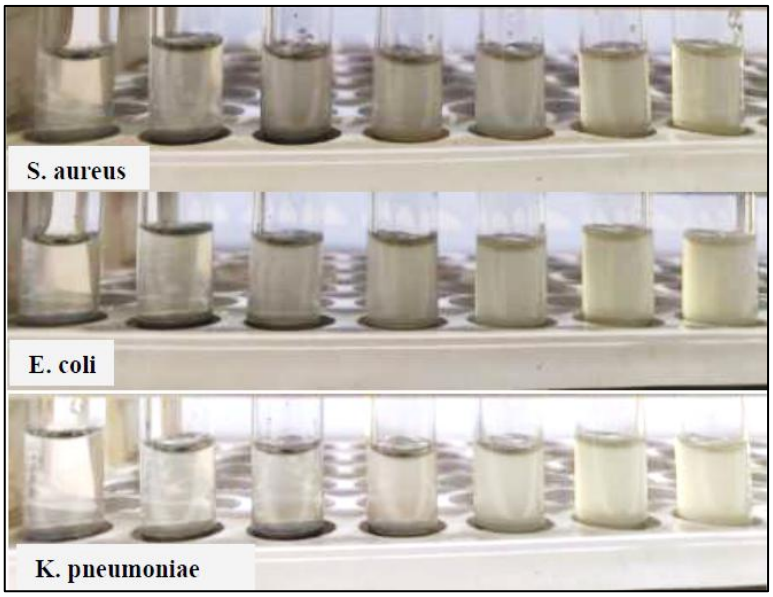

Fig. 5. Photographic views of the antibacterial tests of Fe_3O_4 NPs with three different microorganisms. Order of the tubes from left to right (100 mg/ml, 50 mg/ml. 25 mg/ml, 12.5 mg/ml, 6.25 mg/ml, 3.125 mg/ml and 1.562 mg/ml, respectively).

Table 1: Minimum inhibitory concentration (MIC) values of Fe_3O_4 NPs for microorganisms.

Microorganism	S. aureus	E. coli	K. pneumonia
MIC (mg/ml)	50	50	25

processes.

Field Emission Scanning Electron Microscope (FESEM)

The FESEM morphologies of the magnetic iron oxide nanoparticles are displayed in Fig. 4. The shape of the Fe_3O_4 nanoparticles is quite homogeneous and almost agglomerated, with a cubical to sub-cubical appearance. Furthermore, some agglomeration is seen in the sample as a result of the strong Van der Waals force and magnetic attraction between the Fe_3O_4 nanoparticles [23]. The majority of the nanoparticles are between 10 and 80 nm in size. Our synthesized sample has an average proportion of nanoparticles of 52.5 nm.

Antibacterial activity of Fe_3O_4 NPs

Table 1 and Fig. 5 show the antibacterial properties of the iron oxide nanoparticle tested against three harmful bacteria (S. aureus, E. coli, and K. pneumoniae). According to the MIC data, the susceptibility profiles of Staphylococcus aureus, E. coli, and K. pneumoniae to Fe_3O_4 NPs varied from left to right (100 mg/ml, 50 mg/ml). The corresponding concentrations were 25 mg/ml, 12.5 mg/ml, 6.25 mg/ml, 3.125 mg/ml, and 1.562 mg/ml. The compound's moderate antibacterial activity against S. aureus and E. coli was shown by their respective MIC values of 50 mg/ml.

On the other hand, K. pneumoniae showed a lower MIC value of 25 mg/ml, suggesting that it was more sensitive to Fe_3O_4 NPs. Various nanoparticles were used in numerous antibacterial investigations. Reactive oxygen species (ROS) produced by certain nanoparticles are the cause of the bactericidal action [29]. The antibacterial activity of Fe_3O_4 may be due to a chemical reaction between hydrogen peroxide and membrane proteins or between the chemical generated in the presence of Fe_3O_4 nanoparticles and the bacterial outer bilayer. Bacteria are killed by the hydrogen peroxide that is created when it penetrates their cell membrane. Additionally, it is seen that when the hydrogen peroxide is produced, the nanoparticles remain in contact with the dead bacteria, preventing additional bacterial activity and causing the production and release of hydrogen peroxide into medium [30].

CONCLUSION

Using the co-precipitation method, a straightforward procedure for creating magnetite iron oxide nanoparticles (Fe_3O_4 NPs) with favorable magnetic characteristics in a single step was effectively completed. When a solid black powder precipitate forms, it may be decanted with a magnet, indicating the production of the magnetic phase Fe_3O_4. FT-IR, XRD, DLS, and FESEM were used to analyze the produced nanoparticles, and the synthesis mechanism of this approach was examined. Absorption peaks in FTIR were found to correspond to Fe_3O_4 vibrations associated with the magnetic phase. The six diffraction peaks in the XRD pattern were linked to the atomic planes (111), (220), (311), (400), (422), (511), and (440). According to the investigation, Fe_3O_4 NPs have a cubic phase crystal structure, with a lattice parameter of a = 8.3060A˚ and an average crystal size of 15.7 nm. According to a diffraction light scattering (DLS) particle size analyzer, the average size of an iron oxide nanoparticle is between 10 and 127 nm. The nanoparticles' average size was 52.5 nm, and the FESEM pictures they generated were cubical to sub-cubical in form. The results of this survey showed that Fe_3O_4 NP had potential antibacterial properties against some bacteria. To precisely understand the mechanics of these nanoparticles, further surveys are required.

ACKNOWLEDGMENT

Authors are grateful to Department of Basic Sciences, College of Dentistry, University of Diyala, Diyala, Iraq for providing laboratory facilities.

CONFLICT OF INTEREST

The authors declare that there is no conflict of interests regarding the publication of this manuscript.

REFERENCES

1. Shaji N, Sukumaran S, Prasad P, Jose J, Thomas S, Kalarikkal N. Water Purification Using Nanoparticles. Nanoparticles

in Polymer Systems for Biomedical Applications: Apple Academic Press; 2018. p. 263-280.
2. Abbas ZMA, Shatti WA, Mohammad AM, Khodair ZT. Magnetic iron oxide: preparation and characterization for antibacterial activity applications. J Sol-Gel Sci Technol. 2023;109(2):534-542.
3. McNamara K, Tofail SAM. Nanoparticles in biomedical applications. Advances in Physics: X. 2016;2(1):54-88.
4. Ghazanfari MR, Kashefi M, Shams SF, Jaafari MR. Perspective of Fe_3O_4 Nanoparticles Role in Biomedical Applications. Biochem Res Int. 2016;2016:1-32.
5. Saqib S, Munis MFH, Zaman W, Ullah F, Shah SN, Ayaz A, et al. Synthesis, characterization and use of iron oxide nano particles for antibacterial activity. Microscopy Research and Technique. 2018;82(4):415-420.
6. Chen Y-T, Kolhatkar AG, Zenasni O, Xu S, Lee TR. Biosensing Using Magnetic Particle Detection Techniques. Sensors. 2017;17(10):2300.
7. Chen Y, Ding X, Zhang Y, Natalia A, Sun X, Wang Z, et al. Design and synthesis of magnetic nanoparticles for biomedical diagnostics. Quantitative Imaging in Medicine and Surgery. 2018;8(9):957-970.
8. McNamara K, Tofail SAM. Nanosystems: the use of nanoalloys, metallic, bimetallic, and magnetic nanoparticles in biomedical applications. Physical Chemistry Chemical Physics. 2015;17(42):27981-27995.
9. Liu Y, Zhu W, Wu D, Wei Q. Electrochemical determination of dopamine in the presence of uric acid using palladium-loaded mesoporous Fe 3 O 4 nanoparticles. Measurement. 2015;60:1-5.
10. Sun S-N, Wei C, Zhu Z-Z, Hou Y-L, Venkatraman SS, Xu Z-C. Magnetic iron oxide nanoparticles: Synthesis and surface coating techniques for biomedical applications. Chinese Physics B. 2014;23(3):037503.
11. Xu J-K, Zhang F-F, Sun J-J, Sheng J, Wang F, Sun M. Bio and Nanomaterials Based on Fe_3O_4. Molecules. 2014;19(12):21506-21528.
12. Oztekin A, Romero C, Nato C, Suleiman M, Nikolov N, Neti S. Thermally Active Concrete and Zero Energy Building Research. Curriculum for Climate Agency: Design in Action: ACSA Press; 2021. p. 120-123.
13. Wu W, Wu Z, Yu T, Jiang C, Kim W-S. Recent progress on magnetic iron oxide nanoparticles: synthesis, surface functional strategies and biomedical applications. Science and Technology of Advanced Materials. 2015;16(2):023501.
14. Yusoff AHM, Salimi MN, Jamlos MF. Critical Parametric Study on Final Size of Magnetite Nanoparticles. IOP Conference Series: Materials Science and Engineering. 2018;318:012020.
15. Massart R. Preparation of aqueous magnetic liquids in alkaline and acidic media. IEEE Trans Magn. 1981;17(2):1247-1248.
16. Rukhsar M, Ahmad Z, Rauf A, Zeb H, Ur-Rehman M, Hemeg HA. An Overview of Iron Oxide (Fe_3O_4) Nanoparticles: From Synthetic Strategies, Characterization to Antibacterial and Anticancer Applications. Crystals. 2022;12(12):1809.
17. Baumgartner J, Dey A, Bomans PHH, Le Coadou C, Fratzl P, Sommerdijk NAJM, et al. Nucleation and growth of magnetite from solution. Nature Materials. 2013;12(4):310-314.
18. Thanh NTK, Maclean N, Mahiddine S. Mechanisms of Nucleation and Growth of Nanoparticles in Solution. Chem Rev. 2014;114(15):7610-7630.
19. Au@MnS@ZnS Core/Shell/Shell Nanoparticles for Magnetic Resonance Imaging and Enhanced Cancer Radiation Therapy. American Chemical Society (ACS).
20. Mahdavi M, Ahmad MB, Haron MJ, Gharayebi Y, Shameli K, Nadi B. Fabrication and Characterization of SiO2/(3-Aminopropyl)triethoxysilane-Coated Magnetite Nanoparticles for Lead(II) Removal from Aqueous Solution. Journal of Inorganic and Organometallic Polymers and Materials. 2013;23(3):599-607.
21. Jasim SK, Hussan SMAA, Noori AS, Habeb AA. Determine surface plasmon resonance and effect parameters laser ablation on Cu and Zn nanoparticles. AIP Conference Proceedings: AIP Publishing; 2024. p. 060008.
22. Jasim SK, Al Hussan SMA, Abd MT. Improving the Mechanical Properties of Dental Fillings by Adding TiO_2 NPs Prepared Laser Ablation. BioNanoScience. 2025;15(3).
23. Light-Mediated Antibacterial Activity of Composites of Polypyrrole and Green Zinc Oxide Nanoparticles Synthesized using Sarcomphalus joazeiro Extract. American Chemical Society (ACS). http://dx.doi.org/10.1021/acsomega.5c03456.s001
24. Rezaei M, Nezamzadeh-Ejhieha A. The ZnO-NiO nano-composite: A brief characterization, kinetic and thermodynamic study and study the Arrhenius model on the sulfasalazine photodegradation. Int J Hydrogen Energy. 2020;45(46):24749-24764.
25. Omrani N, Nezamzadeh-Ejhieh A. Focus on scavengers' effects and GC-MASS analysis of photodegradation intermediates of sulfasalazine by Cu2O/CdS nanocomposite. Sep Purif Technol. 2020;235:116228.
26. Yew YP, Shameli K, Miyake M, Kuwano N, Bt Ahmad Khairudin NB, Bt Mohamad SE, et al. Green Synthesis of Magnetite (Fe_3O_4) Nanoparticles Using Seaweed (Kappaphycus alvarezii) Extract. Nanoscale Research Letters. 2016;11(1).
27. Golabiazar R, Omar ZA, Ahmad RN, Hasan SA, Sajadi SM. Synthesis and characterization of antibacterial magnetite-activated carbon nanoparticles. Journal of Chemical Research. 2019;44(1-2):80-87.
28. Behera SS, Patra JK, Pramanik K, Panda N, Thatoi H. Characterization and Evaluation of Antibacterial Activities of Chemically Synthesized Iron Oxide Nanoparticles. World Journal of Nano Science and Engineering. 2012;02(04):196-200.
29. Abdullah SS, Ahmed FL, Jasim S. Structural and optical studies on sliver nitrate doped polymer blend and effect on some pathogenic bacteria. Revista Mexicana de Física. 2025;71(4 Jul-Aug).
30. Parveen S, Wani AH, Shah MA, Devi HS, Bhat MY, Koka JA. Preparation, characterization and antifungal activity of iron oxide nanoparticles. Microb Pathog. 2018;115:287-292.